

Measurements and linearized models for golf ball bounce.

Stanisław W. Biber^{†,1}, Kristian M. Jones², Alan R. Champneys¹, Riku Green¹, and Robert Szalai¹

¹Department of Engineering Mathematics, University of Bristol, BS8 1TW, UK

²Equipment Standards, R&A Rules Ltd., St Andrews, Fife, UK

[†]Corresponding author: s.biber@bristol.ac.uk

February 7, 2023

Abstract

A detailed set of experiments are described that capture over a 1000 different instances of the bounce of a golf ball. Video analysis is used to capture velocity and spin immediately prior to and subsequent to each bounce for a wide variety of landing conditions. Data are presented from two different turfs; one artificial and one from a typical tee. Measurement errors and repeatability are analysed. The data are compared to predictions from models of rigid bounce with friction, including Penner's modification to account for elasto-plasticity. Coefficients of restitution and friction, and Penner's effective contact angle are fit from the data. A better fit to the data is found using a non-physical piecewise-affine landing to lift-off relationship, which distinguishes between cases that bounce in pure slip from those that undergo rolling. Nevertheless, even balls that undergo rolling are typically found to lift off slipping, having undergone spin reversal. The findings suggest that further effort needs to be spent on finding simple physics-based models of golf-ball bounce.

Keywords: Experimental data collection, golf ball bounce, elasto-plastic bounce

1 Introduction

After the impact between club face and ball, the golf shot can be divided into two main components; the free-flight phase, and the bounce and roll phase. While ball flight is relatively well understood [13], there remains much uncertainty and a paucity of data against which to fit a model for the bounce of a golf ball.

Elementary models of ball bounce are based on Newtonian restitution theory, which assumes an instantaneous, rigid bounce during which kinetic energy is dissipated by a constant factor r^2 , see e.g [6]. In many ball sports, such as tennis, football or cricket, and indeed for the launch of a golf ball from a club face, such approaches can be improved by modelling an elastic ball that has finite contact time with a rigid surface, see e.g. [3, 4, 5, 8].

For the interaction between golf ball and turf, however, the ball remains relatively rigid whereas the turf exhibits elasto-plastic behaviour. A simple modification to the rigid bounce theory to account for such interactions is that due to Penner [12] who argues that the elastoplastic forces during contact are equivalent to the bounce against a rigid surface rotated through an angle β . Based on limited data, Penner proposed a general formula for calculating such an angle, which depends linearly on the inbound angle and speed. Nonetheless, the physical rationale behind it would appear questionable.

Haake [9] presented the largest data set on golf ball bounce that we are aware of in the public domain. More than seven hundred measurements were taken, including different in-bound conditions and at different golf courses. These data were used to examine the effectiveness of different viscoelastic models of golf ball bounce. A two-layer system of springs and dampers was found to show best agreement with the experimental data, yet it was unable to predict all features of lift-off accurately. Also, the two-layer model has many

parameters, not all of which are physically amenable. Subsequent models have typically been evaluated against rather less data, and are thus limited in their predictive power.

To advance understanding of modern golf ball bounce and to motivate a new generation of more accurate models (see, e.g. [1] which includes tangential as well as normal compliance), it has become clear more accurate data is required. As a consequence, we have collected new data on the the motion of a golf ball, immediately before and after impact, over a wide range of inbound speed, angle and spin conditions, using state-of-the art image analysis, not available at the time of Haake’s work. We also attempt a systematic treatment of the effects of measurement error and variability. The results are presented for two different ground types; an artificial and a natural turf. We shall also examine whether these data are consistent with rigid-bounce models, either with or without Penner’s effective slope angle.

The rest of the paper is outlined as follows. Section 2 explains the methods of our study, including experimental set up, data analysis and how we fit the models used for comparison purposes. Section 3 contains the results, which are discussed in Section 4.

2 Methods

2.1 Experimental set up

Two experimental campaigns were performed. In both cases a modern, multi-piece golf ball, as used on the professional tours, was fired from a modified baseball launcher aimed downwards towards the designated surface. The ball was positioned in the launcher between two spinning wheels – one at the top and one at the bottom. The spin speed of each wheel is controlled independently. Variations of these speeds (including possible reverse spin of the upper wheel) allowed a full range of realistic speeds and spins of the golf ball to be attained, and adjustment of the incline of the launcher allowed variation of the landing angle. The wheels of the launcher were aligned so that the axis of the spin imparted on the ball was perpendicular to its plane of motion; thus avoiding any significant side-spin on the ball.

During the first campaign (A) the ball was bounced off a premium artificial golf teeing turf, 30 mm thick, adhered to a rigid surface (wood with a thickness of 38 mm). In the second campaign (B) the ball was bounced off a well-maintained teeing area. In both campaigns, the launcher was moved between each repeat, so that the ball hit a different, undamaged piece of the surface for each recorded impact.

On leaving the launcher, a high speed camera was triggered manually or by a laser sensor to capture a video of the bounce. The recording was made using a Phantom VR603 high speed camera, recording at between 5,000 and 10,000 frames per second. The camera was set to align the image plane with the plane

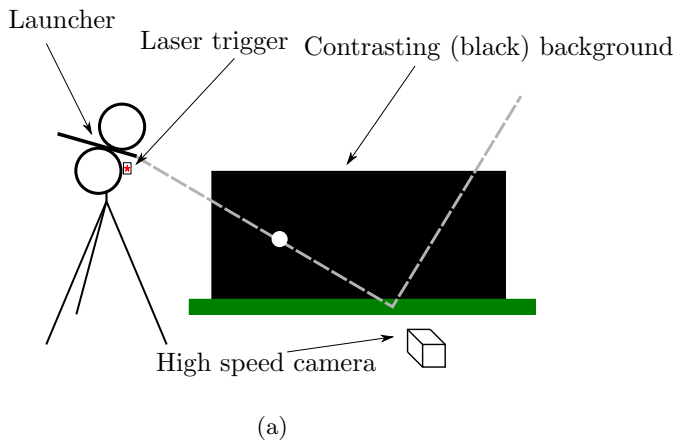


Figure 1: Experimental set up. The ball was launched from a modified baseball launcher. On leaving the launcher, the ball triggered a laser sensor which in turn activated a high-speed camera. (a) Annotated schematic drawing of the setup. (b) Photograph from the experimental session.

of motion of the ball. Each video clip consists of a number of frames prior to and subsequent to the bounce. A superposition of frames from one such clip is shown in Figure 2a.

For the purposes of automated tracking, the bounce was recorded against a plain black background. Furthermore, each ball was marked with a line along its seam and dots placed in a regular array around this seam. Videos were taken outdoors, in summer, for which natural lighting proved to be sufficient.

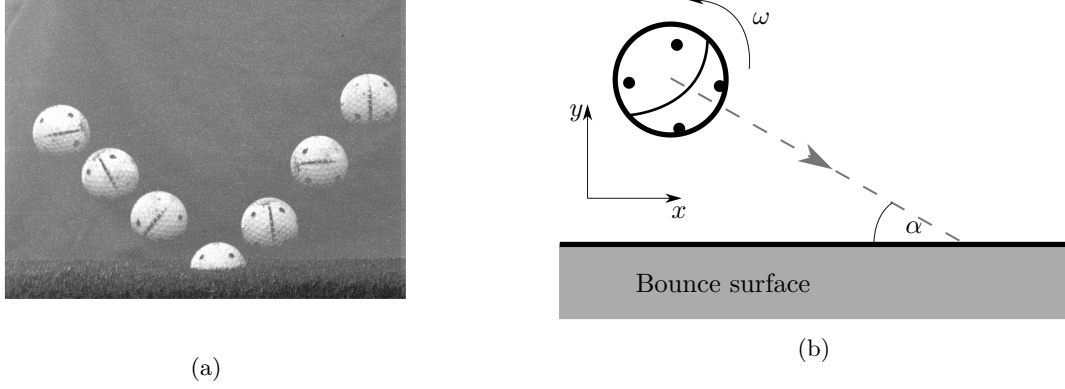


Figure 2: Left: A combination of frames recorded for a single bounce. Time intervals between frames vary and are chosen only for ease of illustration. Right: Definition sketch of the variables used throughout the analysis of the data.

The settings on the launcher (wheel speeds and launch angle) were chosen to span a wide range of conditions typical to golf. Ball bounces for each setting of the launcher were repeated 6 times in Campaign A and either 6 or 12 times in Campaign B. A total of 330 bounces were recorded in Campaign A and 693 in Campaign B.

2.2 Landing conditions

The variables used to define the ball's landing conditions are given in Figure 2b. Note that y is measured vertically upwards, meaning that landing velocities \dot{y} will always be negative, and the spin ω is measured anti-clockwise; thus $\omega > 0$ represents backspin and $\omega < 0$ topspin. To provide consistent and comparable measures of error, we use scaled units that give approximately comparable values for linear and rotational velocity; thus, x and y are measured in units of ball radii and ω in radians per second.

Table 1 presents the span of the landing conditions, both in unscaled and scaled co-ordinates. The full

Table 1: Range of initial conditions for Campaigns A and B

Campaign A					
DIMENSIONAL QUANTITIES			SCALED QUANTITIES		
	min	max		min	max
Speed [m s^{-1}]	6.35	56.1	\dot{x} [s^{-1}]	74.9	2260
Angle of incidence α [deg]	18.3	76.4	\dot{y} [s^{-1}]	-1880	-225
Spin [rot per min]	-3750	9100	ω [rad s^{-1}]	-392	953
Campaign B					
DIMENSIONAL QUANTITIES			SCALED QUANTITIES		
	min	max		min	max
Speed [m s^{-1}]	1.93	38.7	\dot{x} [s^{-1}]	1.10	1720
Angle of incidence α [deg]	16.4	89.5	\dot{y} [s^{-1}]	-1570	-90.0
Spin [rot per min]	-3880	16200	ω [rad s^{-1}]	-407	1670

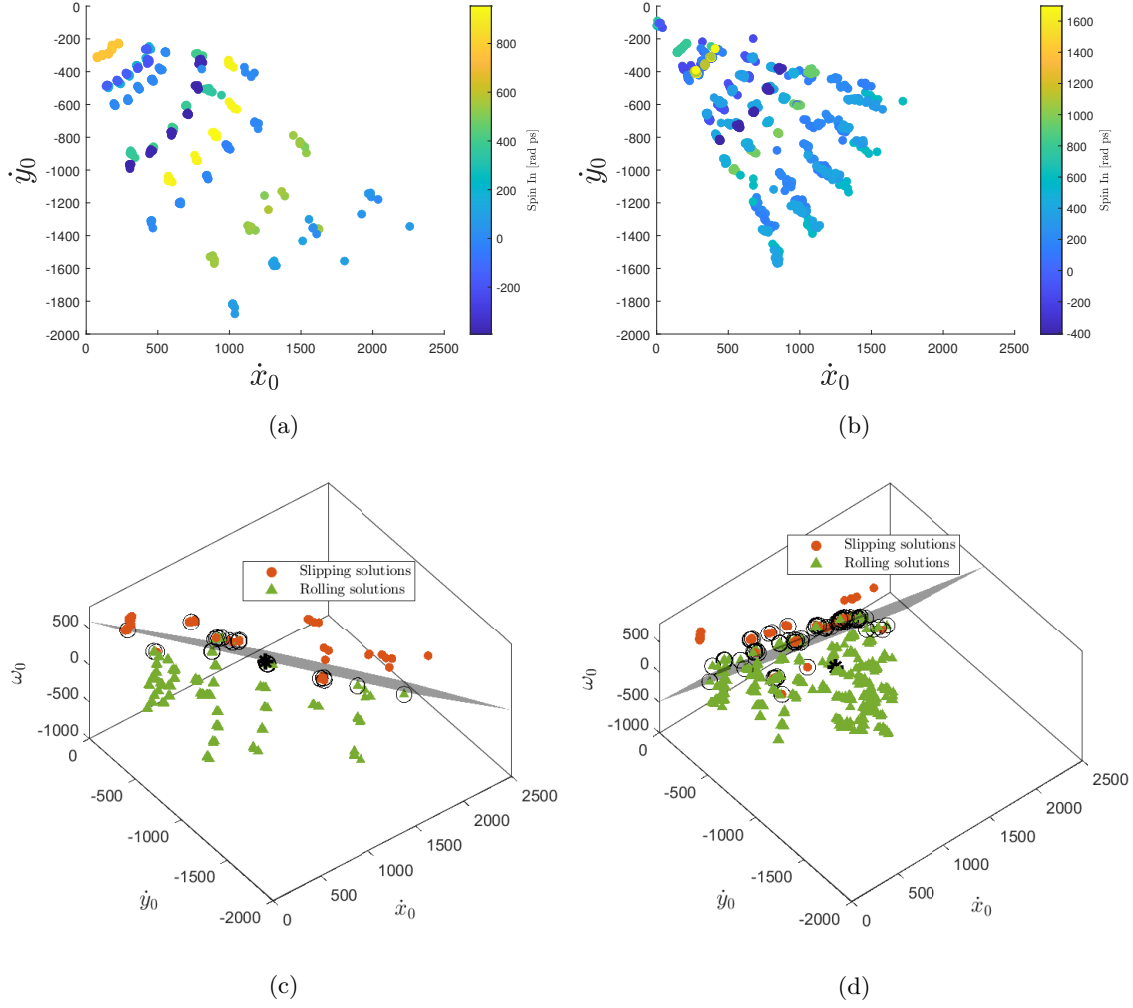


Figure 3: An overview of the landing conditions for (a) Campaign A and (b) Campaign B. (c,d) Corresponding categorisation of the data based on the tangential velocity at lift off their initial conditions for (c) Campaign A; (d) Campaign B. Circled are the boundary data points used for identifying the separating hyperplane. The black asterisk marks typical landing conditions from a tee shot with a driver; speed 93.6 feet per second, landing angle of 37.3° and a backspin of 34.9 revolutions per second.

range of the initial condition space can be seen in Figure 3 for each campaign. The data appears clustered as a result of discrete dials used to control the launcher’s settings.

2.3 Data extraction

A bespoke procedure was developed in MATLAB [11] for the extraction of data from the videos. First, the ball was located in each frame (and frames where the ball was not found were removed from consideration), using the circle detection function `imfindcircle` which is based on the Hough transform [10]. From the change in co-ordinates of the centre between frames, the x and y velocities were established. Second, for each frame, a reduced image was taken, centred around the ball, with a small margin around it. We then used MATLAB’s `extractFeatures` and `matchFeatures` functions to respectively identify significant features to match them between frames. This, in turn, allowed us to construct a 2D rotation matrix to estimate the degree of rotation between frames. Although automated, it was typically found that the black dots on the ball were the mostly commonly extracted and matched features.

In all cases, contact of the ball with the surface occurred over a duration of many frames. The initiation

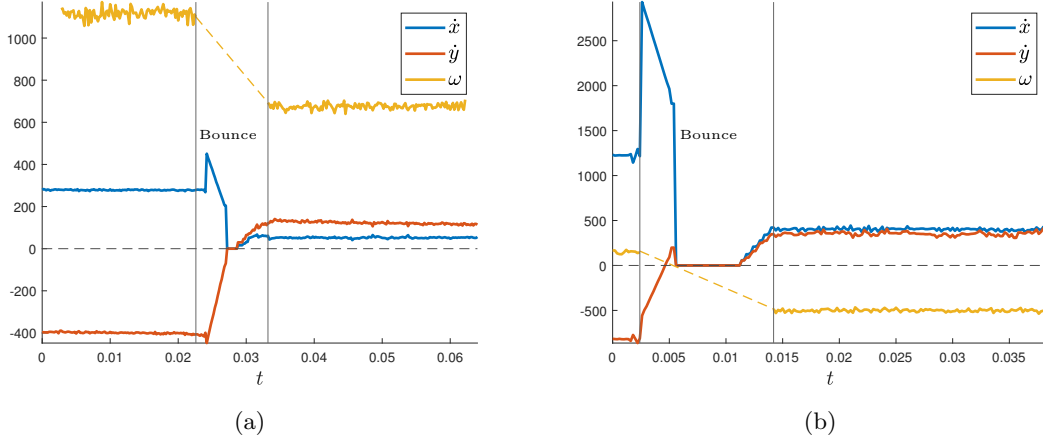


Figure 4: Unprocessed tracing data of a ball prior, during and after bounce for two different launch conditions.

and end time of a bounce was estimated from the identification of abrupt changes in velocity of the lowest visible point of the ball. Also, during bounce, the view of the ball is obstructed by the turf, and locating the ball in the frame and estimating its spin became unreliable (see e.g. Figure 4). For that reason, we decided to restrict the ball bounce analysis to inbound and outbound conditions, just prior and subsequent to the bounce.

2.4 Data analysis

Each bounce was categorised using six quantities; the horizontal velocity, vertical velocity and spin for both touch down (denoted as \dot{x}_0, \dot{y}_0 and ω_0 respectively) and lift-off (\dot{x}_F, \dot{y}_F and ω_F respectively).

2.4.1 Measurement error

As indicated in Fig. 4, the data extracted was not a single point measurement of each velocity and spin, but a noisy time series of measurements for each variable; evaluated at times t_1, t_2, \dots, t_N , where the time interval $\Delta t = t_{i+1} - t_i$ is the frame rate, and is constant for all $i = 1, \dots, N - 1$. For the ball velocities, we used the line of best fit to the derivatives of the position measurements. That is, for the horizontal velocity we found

$$v_x(t) = m t + c \quad (1)$$

such that

$$\varepsilon_x = \sum_{i=1}^{N-1} \left| \frac{x_{i+1} - x_i}{\Delta t} - v_x(t_{i+1}) \right|^2 \quad (2)$$

is minimised. The vertical velocity estimate, $v_y(t)$, was calculated similarly. Incorporating a linear fit accounted for possible effects of the acceleration, such as gravity in the case of the vertical velocity or drag in the case of the horizontal velocity. Parameters m and c were estimated together with their 95% confidence intervals (CI), which then yielded the 95% prediction intervals (PI) for the values of v_x and v_y evaluated at the time of impact or lift-off. The size of the PI gives a parsimonious estimate of measurement error for each velocity in each trial.

It was found useful to treat spin differently, as no evidence of linear changes in spin was found during the recorded short time intervals before and after bounce. We thus assumed that recorded spin in each interval follows a normal distribution, with the noise attributed to measurement error. A normal distribution was thus fit to time series for each spin measurement and the mean of this distribution taken as the measured spin. The 95% CIs of the mean is thus taken as the PI for spin.

2.4.2 Repeatability

Alongside estimates of measurement error provided by the PI for each launch, using 6 or 12 repetitions for each launching setting enabled a check on whether the tests recorded with similar initial conditions led to similar outbound measurements. For each test condition, the mean and 95% CI's on the mean were calculated for each quantity (horizontal velocity \dot{x} , vertical velocity \dot{y} and spin ω), both on their inbound and on outbound measurements. A larger width of each CI shows a larger spread of data around the mean and less repeatability in that quantity.

2.4.3 Distinguishing between slipping and rolling

The tangential velocity of the lowest point of the golf ball should carry information about the frictional dynamics of the ball. If the velocity of this point is zero, the frictional interface will be in a state of 'stick' which suggests that the ball is rolling for a time. In contrast, a non-zero tangential velocity suggests that the ball is 'slipping' against the surface. Denoting such a point as P , in the scaled variables, the tangential velocity of P is given by

$$v_P = \dot{x} + \omega. \quad (3)$$

We separated the initial condition space into two groups, based on the measurement of the tangential velocity of P at touch down and at lift off. If the tangential velocity were of the same sign at touch down and lift-off (non-zero in each case) then it was deemed that the ball was **slipping** throughout the bounce. In all other cases, we deduced that the ball must have entered **rolling** at some point during the bounce.

To identify a possible separation manifold between these groups, a support vector machine (SVM) classifier was trained using the sequential minimal optimisation (SMO) algorithm [7]. The trained SVM identified the data points at the boundary between the two classes, and these were used to identify the surface separating the landing condition space into the subspaces generating the rolling and slipping trajectories. On experimentation (and using insights obtained with models in [1]), we found that the boundary was well approximated by a plane within landing condition space, for the range considered.

2.5 Comparison with existing models

A key aim of this paper is to compare the data with some of the most commonly used models in the literature.

2.5.1 Rigid-bounce model

The simplest model (e.g. [6]), assumes that the bounce is instantaneous and results in a proportional loss of normal velocity, with the ratio

$$r = |\dot{y}_0/\dot{y}_F|, \quad (4)$$

known as Poisson's coefficient of restitution. Further, Coulomb friction is assumed to act between the ball and the surface, with a constant coefficient μ , such that the ball is

$$\text{slipping when } |\lambda_T| = \mu\lambda_N \text{ and rolling when } |\lambda_T| < \mu\lambda_N,$$

where λ_T and λ_N denote the respective tangential and normal forces acting on the point P . The model thus consists of two parameters, μ and r , which are properties of the bounce surface. Typically $0 < r < 1$, $0 < \mu < 1.5$

Depending on whether the ball enters rolling or slips throughout the impact, the lift-off values predicted by the model are easily found to be

$$\begin{aligned} \dot{x}_F &= \dot{x}_0 + \mu(1+r)\dot{y}_0, & \dot{y}_F &= -r\dot{y}_0 & \omega_F &= \omega_0 + \frac{5}{2}\mu(1+r)\dot{y}_0 & \text{if } -\frac{\dot{x}_0 + \omega_0}{\dot{y}_0} > \frac{7}{2}\mu(1+r); \\ \dot{x}_F &= \frac{5}{7}\dot{x}_0 - \frac{2}{7}\omega_0, & \dot{y}_F &= -r\dot{y}_0 & \omega_F &= -\frac{5}{7}\dot{x}_0 + \frac{2}{7}\omega_0 & \text{if } \left| \frac{\dot{x}_0 + \omega_0}{\dot{y}_0} \right| < \frac{7}{2}\mu(1+r); \\ \dot{x}_F &= \dot{x}_0 - \mu(1+r)\dot{y}_0, & \dot{y}_F &= -r\dot{y}_0 & \omega_F &= \omega_0 - \frac{5}{2}\mu(1+r)\dot{y}_0 & \text{if } -\frac{\dot{x}_0 + \omega_0}{\dot{y}_0} < -\frac{7}{2}\mu(1+r). \end{aligned} \quad (5)$$

The parameters μ and r were fit from the available data using a structured approach. First, the coefficient of restitution was found using a least-squares approach applied to each measured inbound and outbound

vertical velocity. Second, a least squares estimate was used again to find μ . Equations (5) were then used to calculate predicted values

$$\mathbf{P}_F^i = [\dot{X}^i, \dot{Y}^i, \Omega^i]^\top \quad (6)$$

for $[\dot{x}_F, \dot{y}_F, \omega_F]^\top$ for each measured landing sample i of incoming values $\mathbf{p}_0^i = [\dot{x}_0^i, \dot{y}_0^i, \omega_0^i]^\top$.

The error of the model for all N samples in a campaign was calculated as:

$$\delta = \frac{1}{N} \sum_{i=1}^N \frac{\|\mathbf{p}_F^i - \mathbf{P}_F^i\|}{\|\mathbf{p}_0^i\|}, \quad (7)$$

where $\mathbf{p}_F^i = [\dot{x}_F^i, \dot{y}_F^i, \omega_F^i]^\top$ are the measured lift-off values and $\|\cdot\|$ represents the usual Euclidean norm of a vector. Note that to be a meaningful error measurement, each component of $\mathbf{p}_0, \mathbf{p}_F, \mathbf{P}_F$ must be of the same order of magnitude, highlighting the importance of working with our scaled velocity quantities. The error measure computed in (7) can be thought of as the root-mean-square error with respect to the initial kinetic energy of the system.

Similarly, we computed the average error for each individual quantity \dot{x}, \dot{y}, ω , (generically denoted as q with a predicted computed value Q) via:

$$\Delta q = \frac{1}{N} \sum_{i=1}^N \frac{|q_F^i - Q_F^i|}{\|\mathbf{p}_0^i\|}. \quad (8)$$

Note that the average quantities computed by (8) neither sum nor average to the error computed by (7) – they are simply an indicator of where the largest error is generated.

A fixed estimate of the coefficient of restitution r for the rigid bounce model was calculated by varying parameter μ , such that the total error, as specified by Equation (7), is minimised.

2.5.2 Inclined surface model

Penner's model [12] was examined in a similar fashion. This model proposes that the bounce of a rigid ball against a horizontal compliant surface can be modelled as the bounce of a rigid ball against a rigid surface that has been rotated by an angle β . The specific formulation proposed in [12] is that

$$\beta = k_P s \phi, \quad \text{where } s = \sqrt{\dot{x}_0^2 + \dot{y}_0^2} \quad \text{and } \phi = \arctan \left[-\frac{\dot{y}_0}{\dot{x}_0} \right]. \quad (9)$$

Here s is the incoming ball speed and ϕ is its landing angle; k_P is a turf-dependent constant.

The model requires fitting parameter k_P , in addition to μ and r . We ran Matlab's genetic algorithm toolbox **ga** to fit all three parameters, minimising the error function (7). The chosen tolerance in minimising the function was 10^{-15} . In each setting, the coefficient of restitution was specified within the frame of reference that is rotated through β .

We explored the idea of the rotated frame of reference in two ways – either the angle of rotation was determined by the initial condition, as specified by (9), or supposing that the angle β is fixed for all initial conditions.

2.5.3 A piecewise-linear data fit

In addition, within each half-space, either side of the boundary between slipping and rolling identified in Section 2.4.3, we attempted to fit an affine transformation. That is, for the measured initial condition \mathbf{p}_0 and outbound \mathbf{p}_F , we approximate the latter with

$$\mathbf{P}_F = A\mathbf{p}_0 + \mathbf{b}, \quad (10)$$

where A is a 3×3 matrix, and \mathbf{b} is a 3-dimensional vector.

To allow for validation of the fit, we separated our data into two categories for each campaign. One data point from each launcher setting (chosen at random) was removed from the general set of data and placed into a testing set, with the remaining data points used for training of the model (10). The testing data set was used to evaluate the accuracy of model (10), using the error measure (7) and (8).

3 Results

The full data set is presented in the Appendix A and is available online [2] along with the full videos. The data set covers a wide range of inbound velocity and spins, and includes examples of backwards bounce, that is where the sign of the horizontal velocity \dot{x} reverses between impact and lift-off.

3.1 Measurement error and repeatability

Figure 5 shows histograms of the widths of the prediction intervals (PIs). These are re-scaled with respect to the average measurement across the samples. That is, a value 1 on the horizontal axis of each histogram would correspond to the average horizontal, vertical or angular velocity on either inbound or outbound across all samples. These PI's provide a parsimonious estimate of the error in measuring speeds via the video analysis.

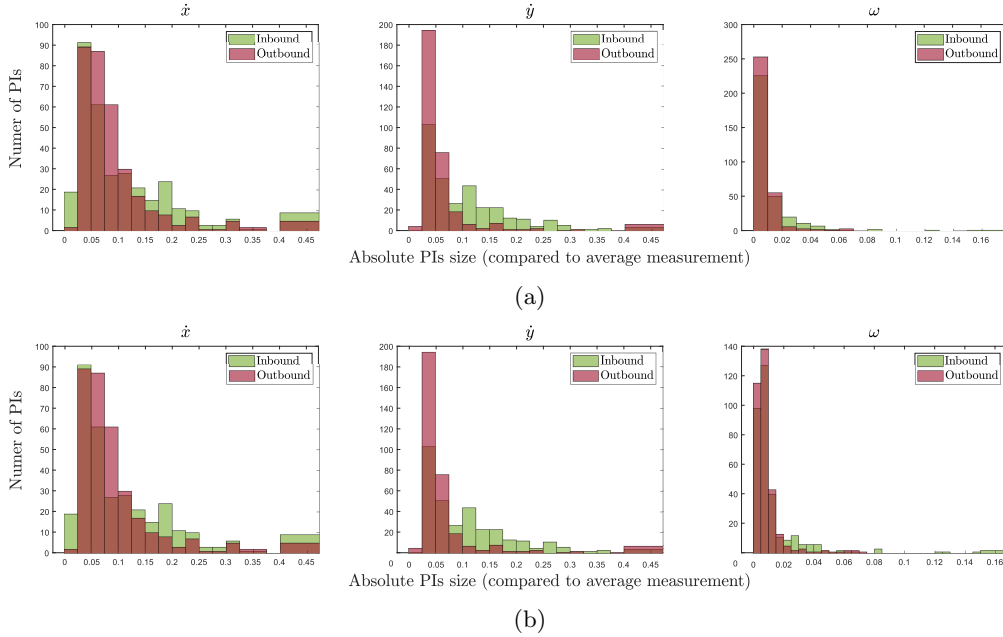


Figure 5: Histogram of widths of PIs in (a) Campaign A; (b) Campaign B. values are rescaled by the average measurement across all samples. From left to right these are for the horizontal velocity \dot{x} , vertical velocity \dot{y} and spin ω . Green bins represent measurements taken on the inbound, red bins represent those taken on the outbound.

In contrast, the repeatability of tests with identical launcher settings is illustrated in Figure 8. Each circle denotes the mean of the respective quantity for a particular test condition, where error bars represent the 95% confidence interval about the mean.

3.2 Piecewise linear model slipping and rolling

Figure 6 presents the tangential velocity v_p of point P at the time of impact and lift off for both campaigns. In particular, observe an offset of lift-off velocities away from zero. That is, balls seem rarely, if ever, to lift off in a state of rolling. There is always some slip at lift off. Furthermore, notice a clear separation between those samples that lift off with positive tangential velocity v_p from those with negative v_p .

The cases with $v_p > 0$ correspond to cases with high initial backspin. In such cases, the ball slips throughout the impact and lifts off with backspin again. Conversely, the cases with $v_p < 0$ at lift-off tend to occur when either the ball landed with high topspin ($v_p < 0$ both at impact and lift-off) or where at some point during the bounce phase the ball entered rolling ($v_p < 0$ initially, but $v_p > 0$ at lift off). It is only the final of these cases that we refer to as a ‘rolling’ trajectory.

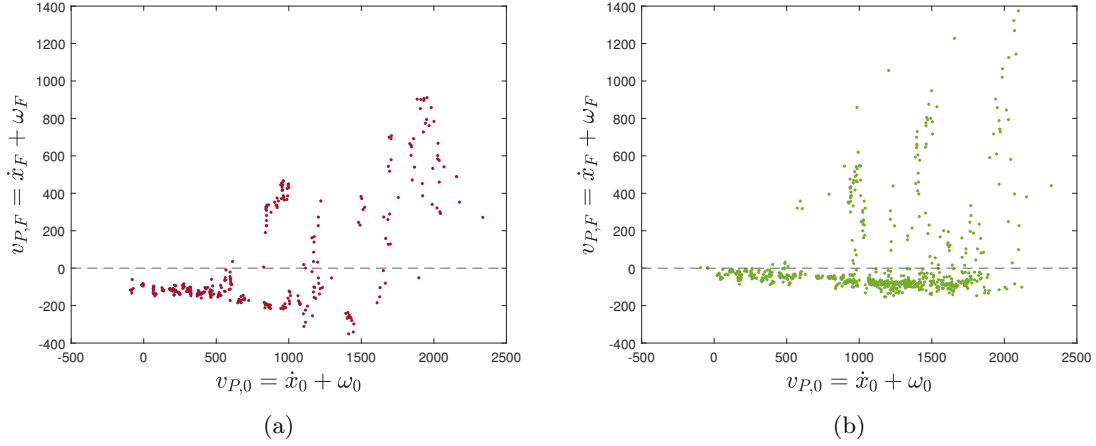


Figure 6: Tangential velocities at landing and lift off. Values for (a) Campaign A; (b) Campaign B. Noted with the dashed line is the zero lift-off tangential velocity.

The distinction between rolling and slipping bounces is visualised in three-dimensional space in Figure 3. For each campaign, the data are separated into different regions of the landing condition space, with only a few data points being mis-labelled by the approximate dividing plane. The boundary cases are identified using the SVM algorithm, and a plane is fitted through the identified boundary points using least squares approximation. Following separation of landing conditions with such a plane, an affine transformation between incoming and outgoing speeds can be identified for each of the subsets.

The resulting fits for Campaign A were:

$$\begin{bmatrix} \dot{x}_F \\ \dot{y}_F \\ \omega_F \end{bmatrix} = \begin{cases} \begin{bmatrix} 0.536 & -0.004 & -0.205 \\ 0.144 & -0.407 & -0.027 \\ -0.524 & 0.091 & 0.318 \end{bmatrix} \begin{bmatrix} \dot{x}_0 \\ \dot{y}_0 \\ \omega_0 \end{bmatrix} + \begin{bmatrix} -111 \\ 23.7 \\ 39.4 \end{bmatrix} & \text{if } 0.891\dot{x}_0 + 0.763\dot{y}_0 + \omega_0 < 600 \\ \begin{bmatrix} 0.674 & 0.107 & -0.005 \\ 0.103 & -0.390 & 0.017 \\ -0.153 & 0.277 & 1.01 \end{bmatrix} \begin{bmatrix} \dot{x}_0 \\ \dot{y}_0 \\ \omega_0 \end{bmatrix} + \begin{bmatrix} -154 \\ 25.0 \\ -267 \end{bmatrix} & \text{if } 0.891\dot{x}_0 + 0.763\dot{y}_0 + \omega_0 > 600; \end{cases} \quad (11)$$

and similarly, for Campaign B the fits were:

$$\begin{bmatrix} \dot{x}_F \\ \dot{y}_F \\ \omega_F \end{bmatrix} = \begin{cases} \begin{bmatrix} 0.326 & 0.222 & -0.213 \\ 0.185 & -0.008 & -0.076 \\ -0.333 & -0.147 & 0.224 \end{bmatrix} \begin{bmatrix} \dot{x}_0 \\ \dot{y}_0 \\ \omega_0 \end{bmatrix} + \begin{bmatrix} 175 \\ 90.4 \\ -171 \end{bmatrix} & \text{if } 0.377\dot{x}_0 + 2.25\dot{y}_0 + \omega_0 < -485 \\ \begin{bmatrix} 0.606 & 0.649 & -0.007 \\ 0.146 & -0.089 & -0.006 \\ -0.192 & 1.01 & 0.887 \end{bmatrix} \begin{bmatrix} \dot{x}_0 \\ \dot{y}_0 \\ \omega_0 \end{bmatrix} + \begin{bmatrix} 117 \\ 49.3 \\ 35.0 \end{bmatrix} & \text{if } 0.377\dot{x}_0 + 2.25\dot{y}_0 + \omega_0 > -485. \end{cases} \quad (12)$$

The support vectors, which identify the boundary data, are highlighted in Figure 3. The error values for the presented fits are given in Table 2. We also present the percentage of testing data that was mismatched following the linear approximation – that is, the percentage of data samples that *a posteriori* are observed to be either rolling or slipping, but the SVM classifier of the space placed them in the wrong category. Furthermore, we present a comparison of the predicted and observed data in Figure 7.

3.3 Rigid-bounce models

The parameters of best fit for the rigid bounce model are presented in the first column of Table 3, for each of the two campaigns. Also given are the fitting errors measured using δ , and $\Delta\dot{x}$, $\Delta\dot{y}$ and $\Delta\omega$ as described in the previous section.

Table 2: Error in the fitting of disjoint linear approximations, as described by Equations (11) and (12).

Campaign A			Campaign B		
	Roll	Slip		Roll	Slip
Overall error δ	6.56 %		Overall error δ	7.84 %	
δ	6.79 %	5.95 %	δ	8.07 %	7.31 %
$\Delta \dot{x}$	4.13 %	3.36 %	$\Delta \dot{x}$	5.33 %	3.76 %
$\Delta \dot{y}$	2.13 %	2.01 %	$\Delta \dot{y}$	2.52 %	0.920 %
$\Delta \omega$	3.94 %	3.59 %	$\Delta \omega$	4.74 %	5.41 %
Mismatched data	7.27 %		Mismatched data	9.59 %	

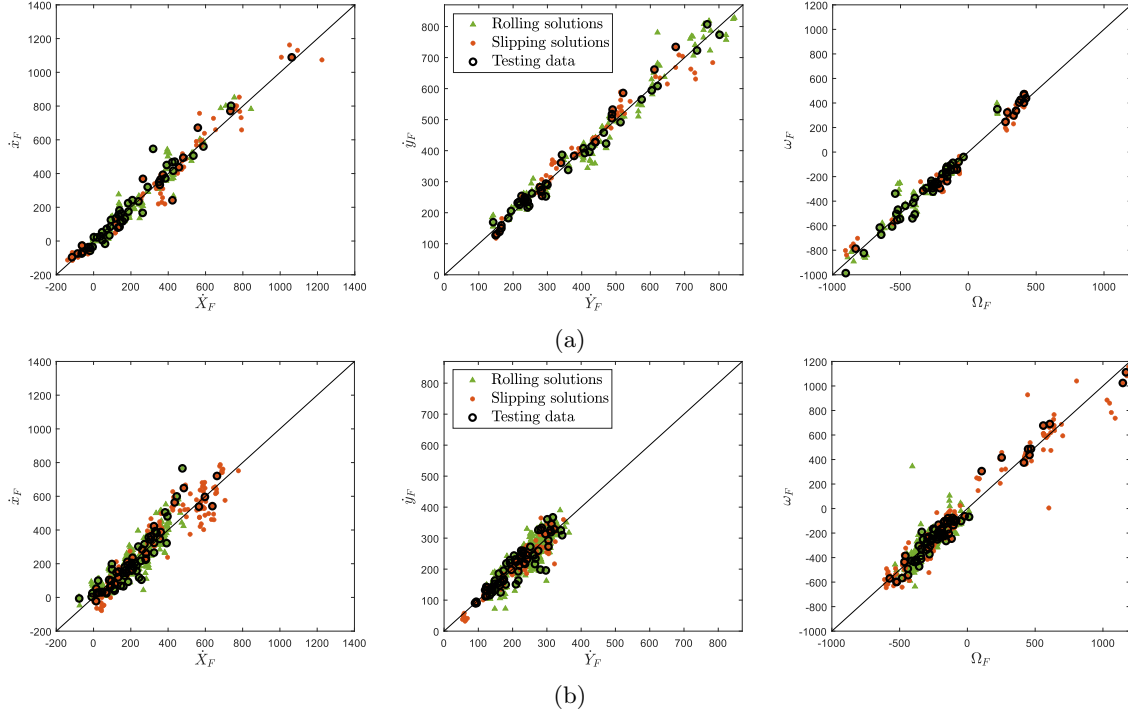


Figure 7: Comparison of the predicted lift off values against the observed results. Solid line indicates the exact fit between prediction and observation. Triangle markers indicate samples classified as rolling, and the circular markers indicate slipping bounces. Marked with black circles are the data samples randomly selected for the testing set to examine the goodness of fits. Data is obtained from (a) Campaign A; (b) Campaign B.

Table 3: Best fit of parameters from each campaign to rigid bounce models, together with the error. See Methods for details.

Campaign A				Campaign B			
	rigid	varying β	fixed β		rigid	varying β	fixed β
β		$k_P = 1.543 \times 10^{-4}$	$\beta = 12.9^\circ$	β		$k_P = 2.973 \times 10^{-4}$	$\beta = 18.4^\circ$
r	0.544	0.448	0.420	r	0.260	0.222	0.147
μ	0.997	0.969	0.852	μ	0.998	0.999	0.998
δ	31.9%	25.5%	19.0%	δ	35.0%	21.3%	19.2%
$\Delta \dot{x}$	19.3%	14.6%	9.58%	$\Delta \dot{x}$	19.8%	9.42%	9.16%
$\Delta \dot{y}$	4.58%	4.42%	3.17%	$\Delta \dot{y}$	6.32%	4.30%	4.24%
$\Delta \omega$	18.6%	16.1%	14.2%	$\Delta \omega$	24.6%	16.4%	15.1%

For Penner’s extension to the model, the results of the fit are presented in the second two columns of Table 3 for each campaign. Observe that the error is slightly smaller than for the simple rigid-body fit, yet still much larger than the SVM fit. Furthermore, the approximation with a constant angle of rotation of the frame β has slightly smaller error than Penner’s proposed approximation linear relationship (9).

4 Discussion

The data presented in this investigation represent the most comprehensive set we of golf ball bounce to data that we are aware of in the open scientific literature. We have taken care to present all steps involved in data collection, curation and error analysis. Using video analysis and modern image processing techniques, we have been able to capture the relationships between the velocity and spin on lift-off to those on landing, for two different turfs. We have also made both this summary data and the raw videos freely available; our purpose being to enable future development and evaluation of physically realistic models of golf ball bounce. As a first step in that process, we have evaluated here three simple models; a plain rigid-bounce model with restitution and Coulomb friction, Penner’s empirical extension to this model, and a simple piecewise-affine fit to the data.

We have also been careful to distinguish the prediction interval of the extraction of each quantity from the video, from the natural variability and repeatability of each measurement. Note that while some of the prediction intervals may appear unrealistically large for a few data points, most prediction intervals are around 5% of the mean value of each quantity. Also, in all cases, we took the mean value from these intervals for performing our data analysis, for which the true error is likely to be significantly smaller.

When looking at the repeatability of the measurements, it is worth noting that in the majority of cases, the confidence intervals on the outbound measurements (horizontal bars in Fig. 8) are wider than those on inbound. This indicates that behaviour of the turf was not fully deterministic; and this points to the variability of turf response. Although present for artificial turf (Campaign A) this effect was less noticeable for artificial turf (Campaign A), which is as expected.

The consideration of tangential velocities at landing and lift-off enabled us to distinguish between slip and rolling, which appears to be key to understanding the dynamics of the bounce of the golf ball. Furthermore, we found little evidence of any ball that lifts off in pure rolling (see Figure 6). Rather, balls that enter rolling during the bounce enter slip in the opposite sense, prior to take-off. In light of this discovery, we postulate that a thorough consideration of different effects of friction and tangential compliance is missing from current models.

It is striking from our model fitting results that the the piecewise-affine fit outperformed both the rigid-bounce and Penner’s models, with overall prediction errors around a factor of five times smaller, for each campaign. As a note of caution, the piecewise-affine model required pre-identification using a SVM of the hyperplane that separates rolling from slipping bounces. Note from that the highest contributions to the error is in the approximation for the outbound horizontal velocity and spin. There is evidence that suggests nonlinear behaviour in these particular variables.

Furthermore, the SVM fit does not provide any insight into the physical principles behind the bounce,

and the fit yields a discontinuous model. Not only is there a non-physical discontinuity in velocity across the slip/roll boundary values discontinuous, but both fits are offset from the origin by a positive value in the \dot{y}_F direction. This would imply that a ball with zero normal velocity (i.e. permanently in contact with flat turf) would spontaneously lift off. This observation provides further evidence that a better model is nonlinear. Such nonlinearity could arise due to a dynamic transition elastic behaviour for low normal velocity and elasto-plastic behaviour for higher speed bounces.

For the rigid bounce model, Table 3 shows that the average error in predictions for the horizontal velocity and spin were beyond reasonable approximation (19.3% and 18.6%, respectively for Campaign A; and 19.8% and 24.6%, respectively for Campaign B). The reason for this poor fit is likely to be due to the rigid bounce model not allowing for any forces other than friction to act in the horizontal direction. Most likely, there is an additional horizontal force due to tangential compliance of the ground. Such effects are explored in [1].

While providing a slightly better fit than the rigid bounce model, Table 3 shows that Penner’s model is still unreasonably inaccurate (14.6% and 16.1%, respectively for Campaign A; and 9.4% and 16.4%, respectively for Campaign B) in the predictions for lift-off horizontal velocity and spin. Note further that using a fixed constant angle β gives a better fit for both campaigns than Penner’s model. Hence, our data does not validate Penner’s model when considering our range of landing conditions.

Furthermore, Figure 6 shows balls lifting off with reversed tangential velocity; a behaviour not possible under the rigid-bounce theory. Penner’s model could qualitatively explain this phenomenon, however we found that no constant of proportionality in Penner’s angle (9) applied to the initial conditions classified as rolling was able to map them to a zero value of v_p . Nor did we find that any constant angle β for that was able to make $v_p \approx 0$ for all such landing conditions.

5 Conclusion

We conclude that a reliable physics-based model of golf-ball bounce is still lacking. Such a model would require a complex nonlinear model of the compliant surface. Most of the discrepancy between the rigid-bounce models and the data are in the tangential and spin degrees of freedom, with error in the normal direction being a factor of five smaller. This observation, along with some of the theoretical conclusions in [1], suggests the need for a combined frictional and tangential compliance model of the turf-ball interaction when studying the bounce of a golf ball. Such models would also need to explain the evidence of nonlinearity we have found in the data.

Acknowledgements

We would like to thank our industrial partner R & A rules Ltd. All experimental work was carried out using R & A’s research facilities. We particularly acknowledge helpful advice from Andrew Johnson and Steve Otto.

Statements and declarations

This work was being partially funded by the EPSRC and by the industrial partner R & A Rules Ltd. The authors have no competing interests to declare that are relevant to the content of this article.

References

- [1] S. W. BIBER, A. R. CHAMPNEYS, AND R. SZALAI, *Analysis of point-contact models of the bounce of a hard spinning ball on a compliant frictional surface*. <https://arxiv.org/abs/2208.11685>, 2022.
- [2] S. W. BIBER, K. M. JONES, AND R. GREEN, *Measurements for golf ball bounce*. Available from University of Bristol Data Repository <https://doi.org/10.5523/bris.1cwnj42n63q5w2sc843iww7bbd>, 2022.

- [3] M. BRAKE, *An analytical elastic-perfectly plastic contact model*, International Journal of Solids and Structures, 49 (2012), pp. 3129–3141.
- [4] M. J. CARRÉ, D. M. JAMES, AND S. J. HAAKE, *Impact of a non-homogeneous sphere on a rigid surface*, Proceedings of the Institution of Mechanical Engineers, Part C: Journal of mechanical engineering science, 218 (2004), pp. 273–281.
- [5] L. P. CORDINGLEY, *Advanced modelling of surface impacts from hollow sports balls.*, Ph.D. Thesis, Loughborough University, (2002).
- [6] C. B. DAISH, *The physics of ball games*, Hodder and Stoughton, London, 1981.
- [7] R.-E. FAN, P.-H. CHEN, C.-J. LIN, AND T. JOACHIMS, *Working set selection using second order information for training support vector machines.*, Journal of machine learning research, 6 (2005).
- [8] H. GHAEDNIA, X. WANG, S. SAHA, Y. XU, A. SHARMA, AND R. L. JACKSON, *A review of elastic-plastic contact mechanics*, Applied Mechanics Reviews, 69 (2017).
- [9] S. J. HAAKE, *An apparatus for measuring the physical properties of golf turf and their application in the field*, Ph.D. Thesis, The University of Aston in Birmingham, (1989).
- [10] P. V. C. HOUGH, *Method and means for recognizing complex patterns*, Dec. 18 1962. US Patent 3,069,654.
- [11] MATLAB, *version 9.11.0 (R2021b)*, The MathWorks Inc., Natick, Massachusetts, 2021.
- [12] A. R. PENNER, *The run of a golf ball*, Canadian Journal of Physics, 80 (2002), pp. 931–940.
- [13] S. J. QUINTAVALLA, *A generally applicable model for the aerodynamic behavior of golf balls*, Science and Golf IV, Routledge, (2002).

A Data

The mean inbound and outbound speeds and spin measured for each trajectory are summarised in Figure 8, in various two-dimensional slices along with the confidence intervals for each measurement.

The complete data for the same quantities (without means and error bars) are presented in all possible two-dimensional slices in illustrated in Figure 9. The complete data set, and the videos from which they were obtained can be freely downloaded from [2].

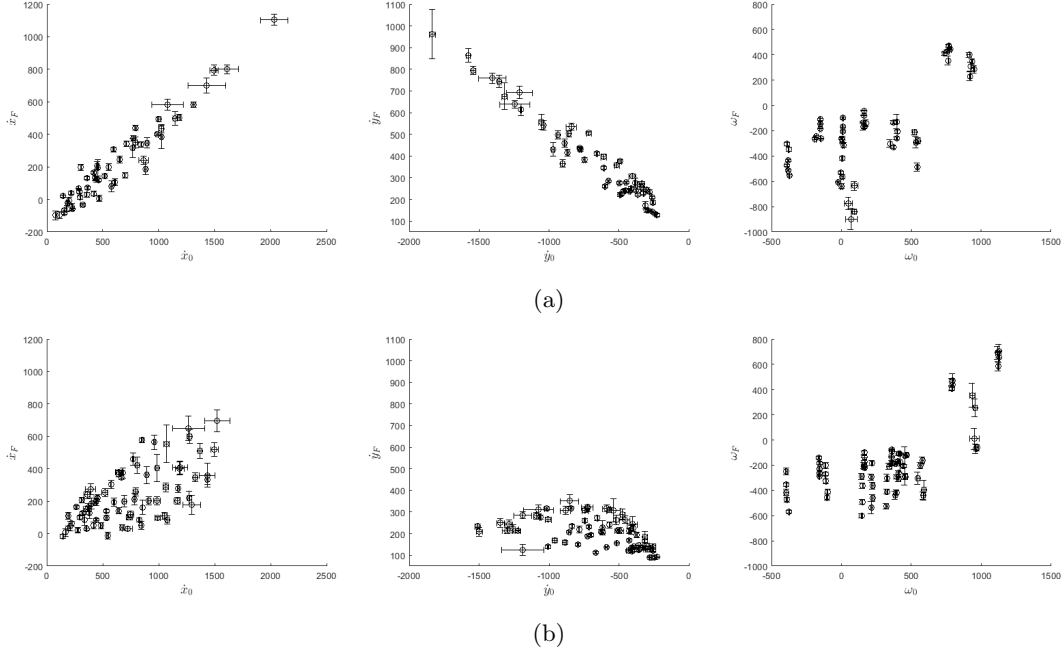


Figure 8: Mean landing and lift-off values for each setting of the launcher (denoted using circles) together with 95% CI of the estimates (denoted using horizontal and vertical error bars). Data is presented for (a) Campaign A, (b) Campaign B; in each case the panels from left to right show horizontal velocity, vertical velocity and spin, respectively.

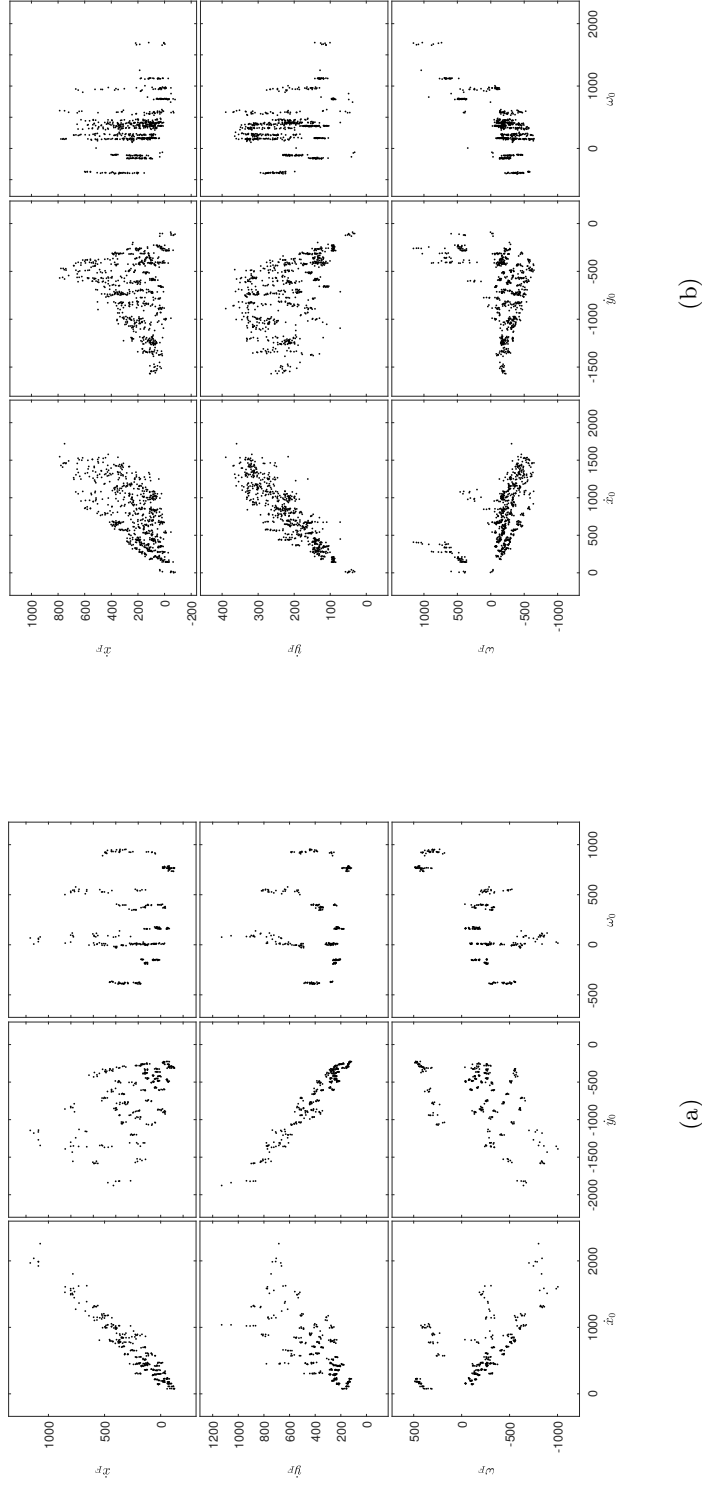


Figure 9: A full representation of all available data from (a) Campaign A; (b) Campaign B. Here, lift off values are presented as the outcome of varying the inbound quantities.